Author for correspondence:
Tali L. Babila
e-mail: t.babila@soton.ac.uk

†Present address: Ocean and Earth Science, National Oceanography Centre Southampton, University of Southampton, European Way, Southampton SO14 3ZH, UK.

Capturing the global signature of surface ocean acidification during the Palaeocene–Eocene Thermal Maximum

Tali L. Babila[1,2,†], Donald E. Penman[1,3], Bärbel Hönisch[4], D. Clay Kelly[5], Timothy J. Bralower[6], Yair Rosenthal[2,7] and James C. Zachos[1]

[1]Department of Earth and Planetary Sciences, University of California Santa Cruz, 1156 High Street, Santa Cruz, CA 95064, USA
[2]Department of Marine and Coastal Sciences, Rutgers, The State University of New Jersey, 71 Dudley Road, New Brunswick, NJ 08901 USA
[3]Department of Geology and Geophysics, Yale University, 210 Whitney Avenue, New Haven, CT 06511, USA
[4]Department of Earth and Environmental Sciences, Lamont-Doherty Earth Observatory of Columbia University, 61 Route 9 W, Palisades, NY 10964, USA
[5]Department of Geoscience, University of Wisconsin-Madison, 1215 West Dayton Street, Madison, WI 53706, USA
[6]Department of Geosciences, Pennsylvania State University, 503 Deike Building, University Park, PA 16802, USA
[7]Department of Earth and Planetary Sciences, Rutgers, The State University of New Jersey, 610 Taylor Road, Piscataway, NJ 08854, USA

(iD) TLB, 0000-0001-9948-9341

Geologically abrupt carbon perturbations such as the Palaeocene–Eocene Thermal Maximum (PETM, approx. 56 Ma) are the closest geological points of comparison to current anthropogenic carbon emissions. Associated with the rapid carbon release during this event are profound environmental changes in the oceans including warming, deoxygenation and acidification. To evaluate the global extent of surface ocean acidification during the PETM, we present a compilation of new and published surface ocean carbonate chemistry and

THE ROYAL SOCIETY
PUBLISHING

pH reconstructions from various palaeoceanographic settings. We use boron to calcium ratios (B/Ca) and boron isotopes ($\delta^{11}B$) in surface- and thermocline-dwelling planktonic foraminifera to reconstruct ocean carbonate chemistry and pH. Our records exhibit a B/Ca reduction of 30–40% and a $\delta^{11}B$ decline of 1.0–1.2‰ coeval with the carbon isotope excursion. The tight coupling between boron proxies and carbon isotope records is consistent with the interpretation that oceanic absorption of the carbon released at the onset of the PETM resulted in widespread surface ocean acidification. The remarkable similarity among records from different ocean regions suggests that the degree of ocean carbonate change was globally near uniform. We attribute the global extent of surface ocean acidification to elevated atmospheric carbon dioxide levels during the main phase of the PETM.

This article is part of a discussion meeting issue 'Hyperthermals: rapid and extreme global warming in our geological past'.

1. Introduction

A hallmark of the Palaeocene–Eocene Thermal Maximum (PETM, approx. 56 Ma) is a negative carbon isotope excursion (CIE) of 3–5‰, signifying a large injection of isotopically light carbon into the atmosphere–ocean reservoirs [1–4]. Although the exact source of carbon is a matter of debate, the event provides a test for our understanding of the ocean's response to the rapid invasion of carbon and heat. The uptake of carbon dioxide (CO_2) in seawater should result in a decrease in ocean pH and calcium carbonate ($CaCO_3$) saturation state (Ω), commonly termed ocean acidification [5]. In the modern ocean, these environmental changes (i.e. warming, deoxygenation and ocean acidification) are connected by a single driver: an increase in atmospheric $p CO_2$ [6]. Current and predicted anthropogenic changes in ocean biogeochemistry inform us that the coastal regions and high latitudes are particularly vulnerable. Changes in continental run-off and nutrient fluxes along with seasonal stratification could amplify pH changes in coastal waters. Southern Ocean waters are inherently low in Ω, making them more susceptible to undersaturation with respect to $CaCO_3$ during ocean acidification events. The geological record can potentially provide insight into the extent to which such environments and their biotas can be impacted by ocean acidification.

The PETM represents a natural experiment of the global ocean response to multiple, covarying environmental stressors. The degree of ocean warming is now well constrained to be 5–8°C [2,7], whereas deep-ocean acidification is largely inferred from widespread dissolution of seafloor carbonate sediments [4,8,9]. Evidence of surface ocean acidification, however, has only recently emerged from planktonic foraminiferal boron isotope ($\delta^{11}B$) and boron/calcium (B/Ca) proxy records [10–12]. Model studies provide ancillary support for whole ocean acidification [13–15]. Marine ecosystems experienced dynamic changes during the PETM but the relative impact of warming, deoxygenation and acidification on organisms remains unclear [16,17]. With improved spatial coverage of boron proxy records, we aim to better constrain the global magnitude of surface ocean acidification.

Here we quantify ocean acidification and its spatial extent within the upper ocean (surface to thermocline) during the PETM, synthesizing new and published records of planktonic foraminifera $\delta^{11}B$ and B/Ca proxies. The study sites span pelagic and coastal environments, and low and high latitudes in the Atlantic and Pacific Ocean basins (figure 1). We generated planktonic foraminifera B/Ca records at high-latitude Southern Ocean (Atlantic Sector, Ocean Drilling Program (ODP) sites 689 and 690) and continental shelf site ODP Ancora, as well as $\delta^{11}B$ data from thermocline-dwelling species at continental shelf sites (ODP sites Bass River and Millville). These new records complement published records from the pelagic, low-latitude Pacific ODP site 1209 [10], continental shelf ODP site Bass River [11] located along the eastern coast of North America and Deep Sea Drilling Project (DSDP) site 401 in the Northeast Atlantic [12]. Seawater properties (temperature, salinity, nutrients and oxygen concentration) and foraminiferal
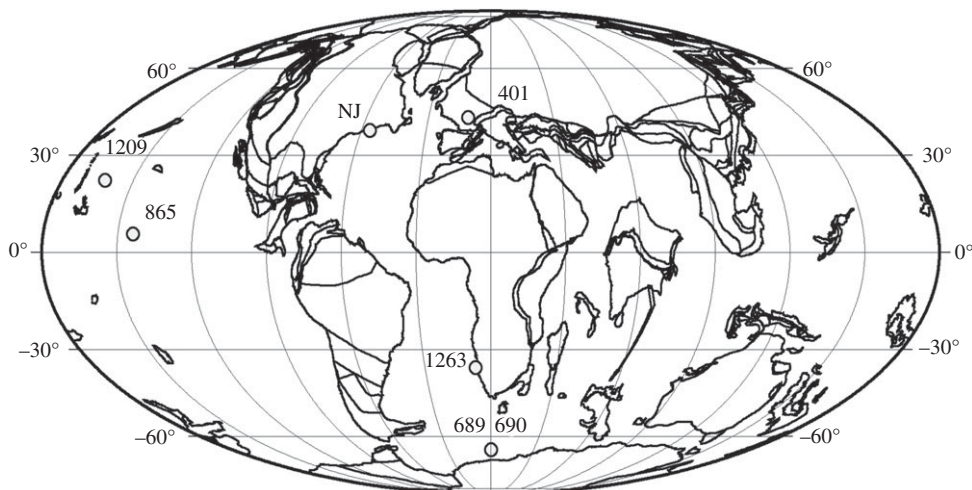
Figure 1. Palaeocene–Eocene (approx. 56 Ma) palaeogeographic reconstruction and core study sites. Pelagic ODP sites include 1209, 1263, 865, 689, 690 and DSDP 401. The map is modified from an Ocean Drilling Stratigraphic Network (ODSN)-generated map using www.odsn.de. New Jersey coastal plain ODP sites include Bass River (BR), Ancora (AN) and Millville (MV).

preservation state vary between the sites, and we exploit these differences to determine the global extent of surface ocean acidification across a diverse range of palaeoceanographic and depositional settings.

2. Methods and material

(a) Site locations and depositional environments

High-latitude pelagic sites 689 (64°31.009′ S, 03°05.996′ E) and 690 (65°9.629′ S, 1°12.296′ E) are located on Maud Rise in the Weddell Sea (figure 1). The PETM palaeodepths of site 689 and site 690, composed of calcareous ooze, are estimated to be 1100 m and 1900 m, respectively [18]. A detailed study has shown that the CIE and its ensuing recovery are preserved within the site 690 PETM section, whereas a coring gap appears to have omitted the upper half of the CIE and the recovery at site 689 [18]. *Acarinina soldadoensis* (250–355 μm size fraction), *A. praepentacamerata* (180–250 μm size fraction) and *Subbotina* spp. (250–355 μm size fraction) were picked from washed sediment samples taken at 1–5 cm resolution at these sites. Because of foraminiferal species assemblage changes during the PETM [19] at sites 689 and 690, *A. praepentacamerata* was measured in the Palaeocene and *A. soldadoensis* was analysed within the CIE interval.

Coastal sites Bass River (BR; 39°36.70′ N, 74°26.20′ W), Millville (39°24.2778′ N, 75°05.3332′ W) and Ancora (39°41.5329′ N, 74°50.9410′ W) are located in New Jersey in the mid-Atlantic coastal plain [20–22] (figure 1). Ancora was closest to the palaeo-coastline, followed by Millville, and the most distal and down-dip site is Bass River, with PETM palaeodepths estimated at 50–150 m, indicative of middle to outer shelf environments [23,24]. These sections are composed of uppermost Palaeocene age micaceous silts and glauconitic sands (Vincentown Formation) transitioning to lower Eocene kaolinitic clay (Marlboro Formation) which yields well-preserved foraminifera tests with glassy textures. This is in contrast to the pelagic sites used in this study, which display a 'frosty' texture indicative of some degree of post-depositional recrystallization.

At Ancora, trace element to calcium ratios were analysed on multi-specimen monogeneric samples of surface-dwelling photosymbiont-bearing *Acarinina* and *Morozovella* spp., and thermocline-dwelling *Subbotina* spp. from the 250–355 μm size fraction to obtain approximately

4

rsta.royalsocietypublishing.org *Phil. Trans. R. Soc. A* **376**: 20170072

200–400 µg of $CaCO_3$ material. The gap in trace element data at the CIE onset (BR: 357.42–357.09 m, AN: 171.59–170.98 m) is due to an absence of foraminifera attributed to carbonate dissolution. At Ancora, resolution is low for the upper Palaeocene, due to low foraminifera abundances. Closely spaced samples were often combined to achieve sufficient sample material for boron isotopes ($\delta^{11}B$) at sites Bass River and Millville. $\delta^{11}B$ measurements were carried out on the few species with adequate abundance, *Subbotina triangularis* (Palaeocene) and *S. roesnaesensis* (Eocene), using the 180–300 µm size fraction to obtain 1–4 mg of $CaCO_3$ material.

(b) Age models

All the sites used in this study have published planktonic foraminifera and bulk carbonate $\delta^{13}C$ records. However, for the purpose of refining age models between sites, we correlate the bulk carbonate records, which benefit from a higher temporal resolution (figure 2*d*). Although the bulk carbonate records differ in magnitude between sites, their temporal $\delta^{13}C$ trends parallel the planktonic foraminiferal records. We provide more details on age constraints for New Jersey and Southern Ocean sites generated in this study in the electronic supplementary material.

(c) Analytical methodology

Trace element analyses were conducted on a Thermo Element XR inductively coupled plasma mass spectrometer at Rutgers University (sites Bass River and Ancora) and the University of California Santa Cruz (ODP 1209, 689 and 690) (figure 2*a–c*). Boron isotopes were measured on a Thermo Triton Thermal Ionization multi-collector mass spectrometer at Lamont-Doherty Earth Observatory (ODP 1209, Bass River and Millville) (figure 3*a*). Foraminiferal cleaning and instrument protocol carried out for records generated in this study (trace elements at sites Ancora, 689 and 690; boron isotopes at sites Millville and Bass River) follow previous work and detailed methodologies are provided therein [10,11].

3. Results

New B/Ca data from sites 689, 690 and Ancora (electronic supplementary material, tables S1 and S2) are presented with published B/Ca records from sites 1209, Bass River and 401 (figure 2*a–c*) [10–12]. At site 690, using *A. praepentacamerata* and *A. soldadoensis* to represent the mixed layer, B/Ca declines by 30% (from 53 to 37 µmol mol^{-1}) within the CIE, then recovers to pre-CIE values (figure 2*b*). *Subbotina* B/Ca, representing the thermocline, is slightly lower throughout but shows a similar 25% decline (from 45 to 34 µmol mol^{-1}) and recovery (figure 2*c*). At site 689, the B/Ca patterns recorded by *A. praepentacamerata*, *A. soldadoensis* and *Subbotina* are similar to those of 690, though slightly offset (figure 2*b,c*). At Ancora, average B/Ca ratios for *Subbotina* spp. decline by 25% (from 51 to 38 µmol mol^{-1}) within the CIE (figure 2*c*). Although no data were generated for the Palaeocene, within the CIE *Morozovella* spp. and *Acarinina* spp. values average 50 µmol mol^{-1} and increase to 70 and 60 µmol mol^{-1}, respectively, in the recovery interval (figure 2*a,b*).

$\delta^{11}B$ data from the Bass River and Millville sites are plotted along with published $\delta^{11}B$ data from sites 1209, 1263, 865 [10] and 401 [12] (figure 3*a*; electronic supplementary material, table S3). Below the CIE onset at site Bass River, average $\delta^{11}B$ values for *Subbotina* spp. are 13.6‰ and decrease to average minimum $\delta^{11}B$ values within the CIE core of 12.5‰ and 12.7‰ at sites Bass River and Millville, respectively (figure 3*a*). To test a potential size bias, $\delta^{11}B$ data were measured in multiple size fractions but no significant offset was found over the size range covered in this study (electronic supplementary material, table S3). This is consistent with data from modern deep dwellers, the ecological parallel of *Subbotina* spp., which show only a negligible $\delta^{11}B$-test size relationship [28].
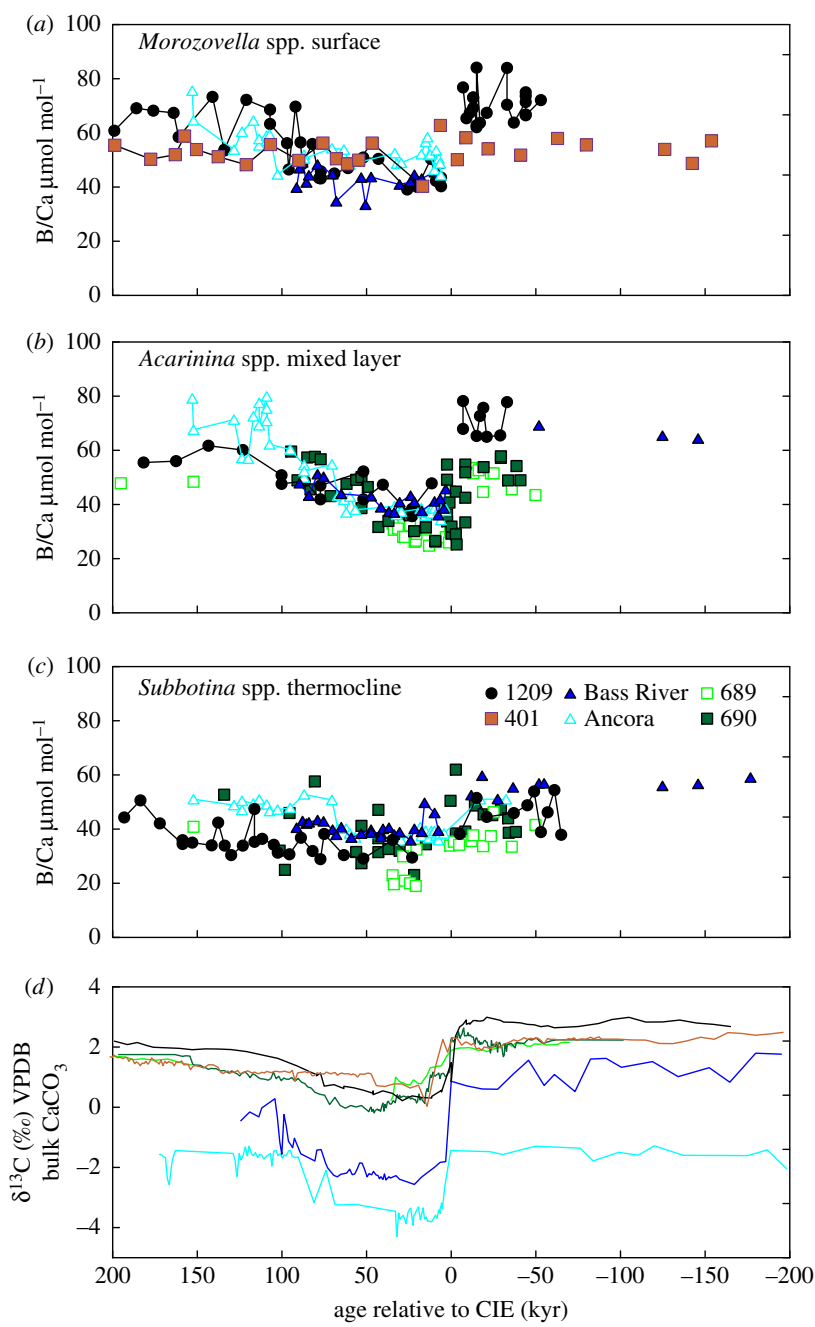
Figure 2. Comparison of planktonic foraminiferal B/Ca (*a–c*) and bulk carbonate $\delta^{13}C$ records (*d*). ODP 1209 (solid black circles) [10], 689 (open light green squares), 690 (solid green squares) and DSDP 401 (solid orange squares) [12] are pelagic sites (*a–c*). ODP sites Bass River (solid blue triangles) [11] and Ancora (light blue triangles) are continental shelf sites (*a–c*). Bulk carbonate $\delta^{13}C$ records (*d*) are labelled in the same colour scheme as B/Ca records (*a–c*). Sites 1209 [9], 401 [12], 690 [25], 689 [18], Bass River [26] and Ancora [27] are plotted versus age in kiloyears relative to the onset of the CIE. A detailed explanation of the age model construction for each site can be found in the Methods section. Analytical reproducibility of B/Ca based on repeated analysis of in-house laboratory consistency standards is 6% and 7% (2 s.d.) at Rutgers University and University of California Santa Cruz, respectively [10,11]. Vienna Pee Dee Belemnite (VPDB) carbon isotope standard. (Online version in colour.)
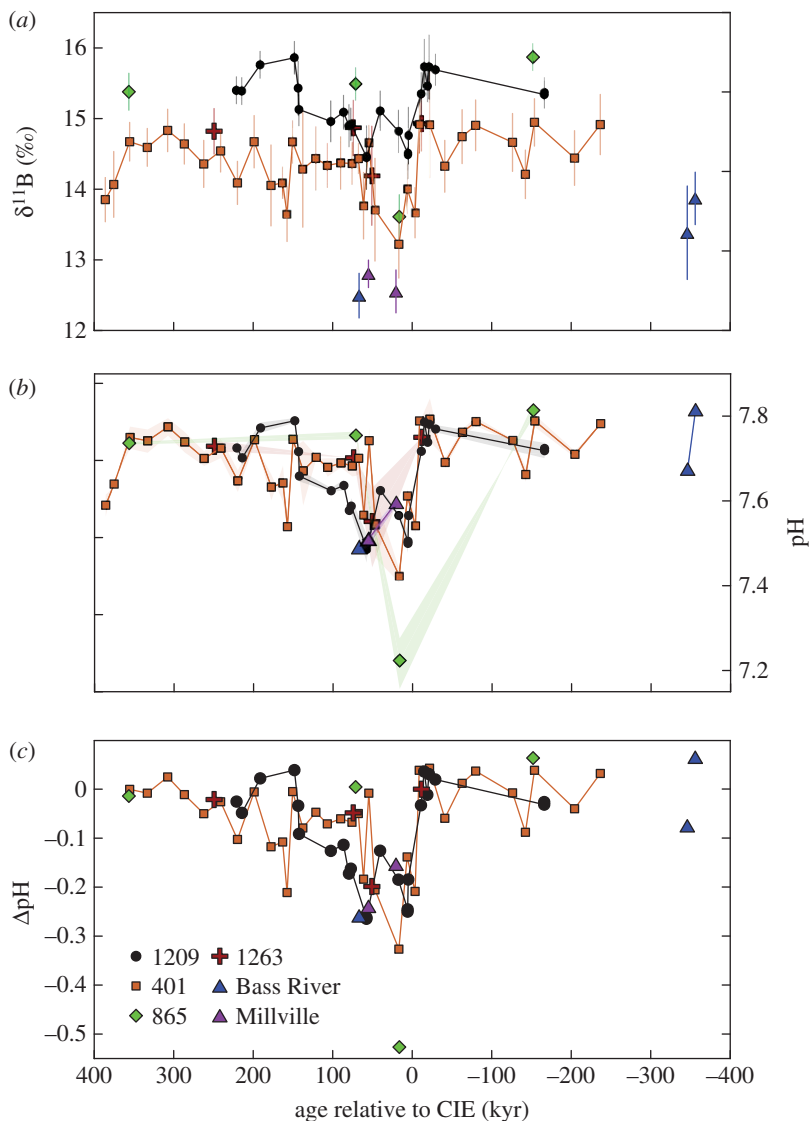
Figure 3. Relative changes in ocean pH derived from planktonic foraminiferal boron isotope (δ^{11}B) measurements (*a*). Surface dweller *M. velascoensis* was used to generate the 1209 (black circles), 1263 (red crosses), 865 (green triangles) [10] and *M. subbotinae* 401 (orange squares) [12] δ^{11}B records (*a*). Deep dweller *Subbotina* spp. were used in δ^{11}B reconstructions at Bass River (blue diamonds) and Millville (purple diamonds) (*a*). All records were normalized to a pre-event ocean pH = 7.75 by adjusting the intercept of the assumed δ^{11}B$_{foram}$ to δ^{11}B$_{B(OH)_4^-}$ calibration following a similar approach to previous studies [10,12] (*b,c*). Ocean pH anomalies ($\triangle$pH) were estimated by computing a relative δ^{11}B change compared with an average of pre-CIE values (*c*). A constant seawater δ^{11}B value of 38.9 $\pm$ 0.4‰ for the duration of the PETM was assumed [12] and no vital effect (δ^{11}B$_{B(OH)_4^-} = \delta^{11}B_{calcite}$) was considered to estimate $\triangle$pH (*c*). Age is denoted in kiloyears relative to the CIE. Error envelopes on ocean pH estimates include the analytical uncertainty of 2 s.e. of repeat sample analyses (*n* = 2–3), and conservative uncertainty estimates for temperature ($\pm$2°C) and salinity ($\pm$2 units) (*b*). (Online version in colour.)

4. Discussion

(a) Global trends in boron proxy records during the Palaeocene–Eocene Thermal Maximum

At all locations, and in each of the three foraminiferal taxa measured, the records follow a common pattern (table 1). Coincident with the onset of the CIE, B/Ca and δ^{11}B decrease, indicating

Table 1. Average planktonic foraminiferal B/Ca and δ^{11}B data during the PETM.

core site	species	average B/Ca μmol mol^{-1a}			$\triangle$B/Ca^b
		below CIE onset	CIE core	post-CIE	
1209	*M. velascoensis*	70.4	44.5	62.7	25.9
1209	*A. soldadoensis*	71.0	43.9	53.5	27.1
401	*M. subbotinae*	51.9	51.4	52.6	0.5
689	*Acarinina* spp.	49.3	29.8	49.2	19.5
690	*Acarinina* spp.	53.4	37.0	52.7	16.4
Bass River	*Acarinina* spp.	65.0	40.0	48.0	25.0
Bass River	*Morozovella* spp.		42.0	45.0	
Ancora	*Acarinina* spp.		38.0	65.0	
Ancora	*Morozovella* spp.		51.0	58.0	
1209	*Subbotina* spp.	46.0	31.3	37.5	14.8
689	*Subbotina* spp.	37.3	24.9	39.2	12.4
690	*Subbotina* spp.	45.3	33.8	42.6	11.5
Bass River	*Subbotina* spp.	57.0	40.0	42.0	17.0
Ancora	*Subbotina* spp.	51.0	38.0	49.0	13.0
		average δ^{11}B (‰)^a			$\triangle\delta^{11}$B (‰)^b
1209	*M. velascoensis*	15.5	14.7	15.3	0.9
401	*M. subbotinae*	14.7	14.0	14.3	0.7
Bass River	*Subbotina* spp.	13.5	12.5		1.1
Millville	*Subbotina* spp.		12.7		

^{a}The onset of the CIE is identified as the initial decrease in δ^{13}C, core CIE is an interval of sustained low δ^{13}C values (less than 70 kyr) and the post-CIE interval represents the recovery of δ^{13}C to values below the CIE onset (70–200 kyr) (figure 2d).
^{b}Difference between average values prior to the CIE onset and the CIE core interval.

acidification of upper ocean waters. In all the boron proxy records that span the duration of the event, this sharp decline is followed by a plateau of consistently depressed B/Ca and δ^{11}B values that persist for approximately as long as the CIE itself (approx. 70 kyr in our age models). Coeval planktonic foraminiferal δ^{13}C values closely track B/Ca records through the CIE onset but δ^{13}C appears to recover faster than B/Ca and δ^{11}B (figures 2 and 3). This could be indicative of decoupling between the key ocean carbonate system parameters (i.e. pH, dissolved inorganic carbon (DIC) and [B(OH)$_4^-$/DIC]) driving each individual proxy [10]. This divergence pattern can be explained by shifting the relative contributions of organic carbon burial versus silicate weathering to carbon sequestration during the CIE recovery. While both processes elevate pH, organic carbon burial is more efficient in raising δ^{13}C because silicate weathering only accelerates dilution of this excess light carbon while organic carbon burial preferentially removes light ^{12}C from exogenic reservoirs. Indeed, geochemical model studies invoke an intensified organic carbon burial feedback to facilitate carbon sequestration during the CIE recovery [12,29]. Finally, near the start of the CIE recovery, B/Ca and δ^{11}B begin to increase coincident with a recovery and temporary overshoot of %CaCO$_3$ in sediments globally [30], including an overshoot in the calcite compensation depth (CCD) [31] and/or a build-up of alkalinity in deep waters [32], suggesting a restoration of carbonate chemistry. Taken together, our foraminiferal boron proxy records support rapid PETM surface ocean acidification from pelagic to coastal, and tropical to polar settings, lasting tens of thousands of years.

A partial exception to the above trends occurs with the geochemical proxy records based on the surface dweller *M. subbotinae* at DSDP site 401 [12]. At site 401, one extreme minimum δ^{13}C point and one extreme minimum δ^{11}B point occur approximately 25 kyr after the CIE onset and are directly followed by the CIE recovery phase (figure 3*a*). Unlike all the other sites, B/Ca at site 401 shows only a very slight decrease at the CIE onset (figure 2*a* and table 1). Furthermore, the foraminifera δ^{13}C records at site 401 exhibit a relatively small CIE magnitude compared with regional and global records [33]. Incomplete recovery by rotary drilling (RCB in International Ocean Discovery Program (IODP) terminology) at site 401 probably resulted in a truncated or disturbed PETM interval [34], which helps explain the discrepancies with other sites [35]. During the recovery of core 401–14R, which contains the PETM, drilling advanced 9.5 m but only 7.2 m of sediment was recovered, indicating the loss of over 2 m of sediment within this interval [34]. Given the abrupt lithological change at the Palaeocene–Eocene boundary, it is likely that at least some of this sediment loss occurred at the base of the PETM, truncating the CIE and associated geochemical records. A similar problem occurred during attempts to recover the clay layer at ODP 1263 by rotary coring [36]. We include the site 401 boron proxy records in the global compilation while recognizing that the CIE is only partially represented (figures 2*a* and 3).

(b) Quantifying changes in seawater carbonate chemistry

Following the approach of Penman *et al.* [10], we use the boron isotope data from mixed-layer and thermocline-dwelling foraminifera to quantify the decrease in surface seawater pH during the onset of the PETM. We focus on the relative magnitude of acidification rather than estimating absolute pH, and use the more established δ^{11}B proxy to corroborate B/Ca trends. Knowledge of past seawater δ^{11}B (δ^{11}B$_{sw}$) as well as a species-specific calibration are required to derive absolute ocean pH using foraminiferal δ^{11}B data. An estimation of temperature, salinity and major seawater ion concentration is also required to calculate the dissociation constant of boric acid (K^{*}_{B}). The experimentally determined boron isotopic fractionation factor of 1.0272 was used [37]. We applied an estimated δ^{11}B$_{sw}$ value of 38.9 ± 0.4‰ [12], which is consistent with δ^{11}B$_{sw}$ estimates over the Eocene [38]. To account for potential laboratory offsets, pre-event δ^{11}B values were normalized to pH = 7.75, following the approach of previous PETM boron proxy model studies [10,12]. K^{*}_{B} was calculated with the MyAMI model assuming Eocene seawater (approx. 50 Ma) [Mg] = 30 mM and [Ca] = 20 mM [39]. Surface and thermocline temperatures are estimated using Mg/Ca palaeothermometry with a modern multi-species calibration [40]. In addition to temperature, variation in past seawater Mg/Ca composition affects the Mg distribution coefficient and possibly Mg/Ca proxy sensitivity to temperature. A nonlinear correction scheme to account for the influence of variable past Mg/Ca$_{sw}$ developed for the modern planktonic foraminifer *Trilobatus sacculifer* was applied to compute ocean temperatures [41]. We used previously generated Mg/Ca records in *M. velascoensis* at site 1209 [10,42], *M. subbotinae* at site 401 [12] and *Subbotina* spp. at site Bass River [11]. Pre- and post-event salinity values of 37 (ODP 1209) and 35 (sites Bass River, Millville and ODP 401) were used and are similar to climate model regional estimates [43]. A salinity increase of 1.5 units was previously determined at site 1209 [42], whereas a 2 unit decrease is estimated for coastal New Jersey sites and a 1.5 unit decrease at site 401 (further discussion on estimation of salinity anomalies in §4c Contribution of regional salinity shifts on B/Ca).

Culture calibration studies with modern planktonic foraminifera document species-specific δ^{11}B$_{foram}$ to δ^{11}B$_{B(OH)_4^-}$ relationships that are variably offset from seawater borate (δ^{11}B$_{B(OH)_4^-}$) values [44]. These isotopic offsets are thought to be caused by the physiological processes of symbiont photosynthesis, respiration and calcification that act to modify pH within the calcifying microenvironment around foraminifera and, subsequently, alter the δ^{11}B recorded in foraminiferal calcite [44]. To estimate ocean pH from the extinct species used in this study, we need to approximate their δ^{11}B$_{foram} - \delta^{11}$B$_{B(OH)_4^-}$ relationships. The first option is to assume equilibrium between δ^{11}B of foraminiferal calcite (δ^{11}B$_c$) and δ^{11}B of seawater borate (δ^{11}B$_{B(OH)_4^-}$), which is equivalent to assuming the absence of any vital effects (δ^{11}B$_c = \delta^{11}$B$_{B(OH)_4^-}$).

Alternatively, habitat ecology (i.e. surface dwelling and photosymbiont bearing) determined by previous studies on the basis of carbon and oxygen isotope offsets can be used as a means to assign a modern calibration relationship to an analogous extinct species. However, ascribing such a modern analogue to an extinct species assumes modern vital effects were similar during the Palaeogene, which is currently poorly understood.

Several lines of evidence argue for diminished vital effects of Eocene age planktonic foraminifera relative to modern species. Reduced δ^{13}C test size relationships in muricate PETM species (acarininids and morozovellids) compared with modern species (*Globigerinoides*) suggest overall lower photosymbiont activity rates [45–47]. If we assume that lower photosynthetic rates translate to reduced vital effects, we would expect foraminiferal δ^{11}B to be closer to seawater $\delta^{11}B_{B(OH)_4^-}$ values. Indeed, δ^{11}B values analysed for a suite of planktonic foraminifera occupying the upper water column show a narrower isotopic range in the Eocene relative to modern day, implying reduced vital effects [38,48]. This is further corroborated by similar δ^{11}B values obtained in time-equivalent Eocene samples of *S. roesnaesensis* and benthic foraminifera *Cibicidoides* [38], genera which are interpreted to have minimal δ^{11}B-related vital effects in modern ocean sediments [44]. When modern ecologically equivalent $\delta^{11}B - \delta^{11}B_{B(OH)_4^-}$ calibration equations are applied to Eocene surface (morozovellids) and thermocline (subbotinids) species, an unrealistic reverse ocean pH depth profile is obtained [38]. This suggests that modern δ^{11}B to $\delta^{11}B_{B(OH)_4^-}$ calibrations overestimate Eocene planktonic foraminifer vital effects. For these reasons, we consider no vital effect ($\delta^{11}B_c = \delta^{11}B_{B(OH)_4^-}$) with a slope of 1.0 to be a closer approximation of surface and thermocline ocean pH change (ΔpH) at the CIE relative to pre-event values (figure 3c). We calculate an average pH decrease for *M. velascoensis* of 0.22 units (extrema 0.12–0.30) at site 1209, 0.15 units (0.04–0.34) for *M. subbotinae* at site 401 and for *Subbotina* spp. 0.22 units (0.23–0.52) in New Jersey (figure 3c). By contrast, if we apply the pH sensitivity of the modern photosymbiont-bearing *T. sacculifer* (slope = 0.82) (refitted in [28,49]) at site 1209, a larger average pH decrease for *M. velascoensis* of 0.26 units (extrema 0.14–0.37) is estimated (electronic supplementary material, figure S1c). Whether we include or exclude any vital effects, our multi-site pH estimates produce a uniform degree of acidification in the coastal ocean compared with pelagic sites (figure 3c; electronic supplementary material, figure S1c) in agreement with model predictions, lending support to our observations [12]. This spatial similarity is perhaps unsurprising, as an increase in atmospheric pCO$_2$ should be absorbed by the surface ocean everywhere, leading to a relatively uniform pH decrease globally. A decline in the degree of surface ocean acidification from the mixed layer to the thermocline is also consistent with model predictions of attenuated acidification with depth [14]. Regardless of the calibration uncertainties, both δ^{11}B records are consistent in providing evidence for upper ocean acidification in support of our interpretation of complementary B/Ca records.

Culturing experiments established a carbonate system control on B/Ca in planktonic foraminiferal calcite [50–53]. A first-order approximation is to simply relate modern B/Ca proxy systematics to interpret PETM records. However, when modern B/Ca calibrations are applied to B/Ca data from extinct PETM taxa, unrealistic negative [B(OH)$_4^-$/DIC] values are estimated [10]. In general, the PETM B/Ca values are significantly lower, extending beyond the modern calibration range. We instead consider new empirical culture calibrations that relate B/Ca to [B(OH)$_4^-$/DIC] of modern photosymbiont-bearing species *Orbulina universa* under simulated Palaeocene seawater chemistry (high [Ca], low [Mg] and low total boron concentration [B$_T$]) [53] (figure 4). We translate B/Ca excursion anomalies (average pre-CIE baseline compared with core CIE values) to estimate Δ[B(OH)$_4^-$/DIC] as in previous studies [10,11] and apply 'Palaeocene'-derived calibration sensitivity [53] (figure 4). We only consider B/Ca excursion anomalies of mixed-layer (acarininids) and thermocline (subbotinids) dwellers, for which there are pre-CIE values recorded at all locations used in this study. We estimate a [B(OH)$_4^-$/DIC] decrease for *M. velascoensis* of 0.023 at site 1209 and essentially no change for *M. subbotinae* at site 401 (figure 4a). For *Acarinina* spp., all sites (NJ, 1209, 689 and 690) show an average decrease of 0.022 (extrema 0.021–0.024) (figure 4b) and *Subbotina* spp. show an average decrease of 0.015 (extrema 0.013–0.018) (figure 4c). Using the new Palaeocene calibration yields [B(OH)$_4^-$/DIC] anomalies are closer
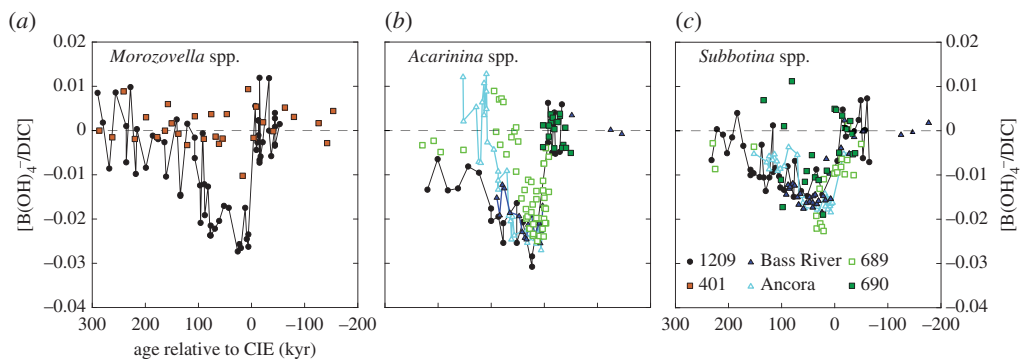
Figure 4. Ocean carbonate chemistry reconstructions derived from planktonic foraminiferal B/Ca records (*a*–*c*). B/Ca records are presented for ODP sites 1209 (black circles) [10], 689 (open light green squares), 690 (solid green squares), Bass River (solid blue triangles) [11], Ancora (light blue triangles) and DSDP 401 (orange squares) [12]. Seawater $[B(OH)_4^-/DIC]$ anomalies are relative to average pre-CIE values and are based on B/Ca — $[B(OH)_4^-/DIC]$ sensitivity determined in modern photosymbiont-bearing planktonic foraminifera species *O. universa* under simulated Palaeocene seawater chemistry [53]. (Online version in colour.)

to previous estimates based on calibrations conducted in modern seawater [10] but still larger than predicted carbonate and borate chemistry estimated by model outputs [53]. This model–data difference could be a result of the Palaeocene calibration being too insensitive to fully resolve the B/Ca anomalies across the PETM [53]. Another explanation is that a larger carbon release (greater than 3000 Pg C) is required to better approximate the B/Ca-based estimates of carbonate chemistry change. Both B/Ca and $\delta^{11}B$ proxies estimate a shift in surface ocean carbonate chemistry towards lower pH and saturation state. Within the calibration uncertainties, both boron-based proxies support a uniform pattern of ocean acidification during the PETM. Coincident biogeochemical changes, such as salinity, dissolution and symbiont loss, could influence B records and we evaluate these factors in addition to seawater carbonate chemistry.

(c) Contribution of regional salinity shifts on B/Ca

Culture experiments reveal a small but significant influence of salinity on boron incorporation and, consequently, B/Ca ratios in planktonic foraminifera [50]. Regional shifts in salinity during the PETM could augment or dampen B/Ca anomalies and, if unaccounted for, bias our interpretation of the B/Ca component related to carbonate chemistry. We can disentangle the influences of salinity and carbonate chemistry by normalizing B/Ca records to a common salinity value. However, accurate estimates of salinity using the paired Mg/Ca-$\delta^{18}O$ method [42] require accurate estimates of temperature and an appropriate $\delta^{18}O_{sw}$–salinity regional relationship, which are difficult to constrain. As an alternative, we chose to reconstruct salinity anomalies relative to pre-CIE baseline values [42]. Morozovellid and acarininid Mg/Ca and $\delta^{18}O$ datasets at sites Bass River [11,26], Ancora [27], 401 [12], 1209 [10,42] and 690 [2,54] were used to estimate relative salinity anomalies. For each site, an average pre-CIE $\delta^{18}O$ and Mg/Ca value was subtracted from each data point to estimate the relative changes across the event, $\Delta\delta^{18}O$ and $\Delta Mg/Ca$. Ocean temperature anomalies were estimated using a multi-species calibration, as inter-species variability in Mg/Ca temperature sensitivity is quite small in modern subtropical planktonic foraminifera [40]. In this way, we can quantify uncertainty of non-thermal controls on Mg/Ca that are necessary to consider for absolute temperature reconstructions. The temperature component of $\Delta\delta^{18}O$ was calculated with a $\Delta\delta^{18}O/\Delta T$ sensitivity of 0.21‰/°C, derived for modern symbiont-bearing *O. universa* [55]. *Orbulina universa* was selected as its temperature sensitivity is a mid-range value for modern planktonic foraminifer species and B/Ca salinity sensitivity is also known [50]. The salinity anomaly estimate assumes the discrepancy between $\delta^{18}O$ and Mg/Ca temperature anomalies is solely from regional surface water $\delta^{18}O_{sw}$. The residual non-temperature $\delta^{18}O$ component corresponds to $\Delta\delta^{18}O_{sw}$ and was converted to ΔSSS
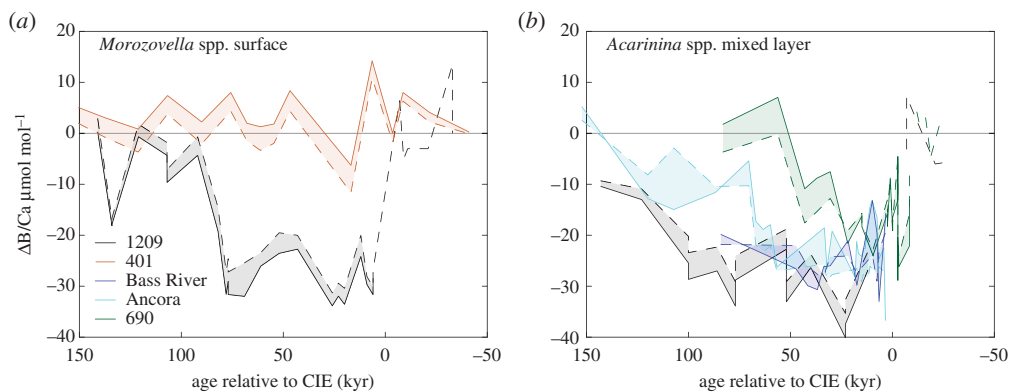
Figure 5. Estimation of the potential contribution of regional changes in salinity to B/Ca records. B/Ca anomalies ($\triangle$B/Ca, μmol mol^{-1}) were computed by subtracting a pre-CIE average value from each point in the record (*a*,*b*). Paired planktonic foraminiferal Mg/Ca and δ^{18}O were used to estimate δ^{18}O$_{sw}$ changes; regional δ^{18}O$_{sw}$–salinity relationships were used to translate δ^{18}O$_{sw}$ to $\triangle$SSS. Plotted here are $\triangle$B/Ca records uncorrected (dashed line) and corrected (bold line) for regional changes in salinity using B/Ca salinity sensitivity of modern *O. universa* derived in laboratory culture experiments [50]. The shaded region represents the potential contribution of local salinity changes to $\triangle$B/Ca records. Age is denoted in kiloyears relative to the CIE. (Online version in colour.)

(surface seawater salinity) by using the same slope as the modern regional $\triangle\delta^{18}$O$_{sw}$ to $\triangle$SSS relationship. The residual $\triangle\delta^{18}$O was converted to $\triangle$SSS using a slope of 0.15‰/SSS at sites Bass River and Ancora [56], 0.38‰/SSS for site 1209 [42], 0.24‰/SSS for site 690 [57,58] and 0.55‰/SSS for site 401 [59].

At each site, the pre-CIE B/Ca average of each species was used as the baseline, and $\triangle$B/Ca was calculated for each sample that also has a paired Mg/Ca and δ^{18}O-based salinity anomaly estimate (figure 5). For *Acarinina* spp., the pre-CIE B/Ca average from site Bass River was applied to proximal site Ancora to compute $\triangle$B/Ca because there are no Palaeocene B/Ca values at Ancora (figure 5*b*). B/Ca records were corrected for $\triangle$SSS using the *O. universa* sensitivity of $\triangle$B/Ca/$\triangle$SSS (2.6 μmol mol^{-1} per salinity unit) as determined in laboratory culture [50]. Both the uncorrected and salinity-corrected $\triangle$B/Ca are shown in figure 5 with the exception of *Morozovella* spp. at sites Bass River and Ancora, as the B/Ca records do not extend into the Palaeocene (figure 2*a*). At the shelf NJ sites Bass River and Ancora, North Atlantic site 401 and Southern Ocean sites 689 and 690 regional salinity decreases amplify the total B/Ca anomaly, while the estimated salinity increase at North Pacific site 1209 dampens the total anomaly. These estimated salinity changes can account for a 13% increase in the total B/Ca anomaly at site 1209, and an 11% and 22% decrease in NJ and Southern Ocean sites, respectively. In our salinity correction on B/Ca, we assume that modern B/Ca salinity sensitivities apply to extinct PETM taxa. This should be considered an approximation because modern studies document species-specific B/Ca salinity responses [50], and it is unclear whether these modern salinity sensitivities might have been different under Palaeocene seawater composition. In light of these assumptions, we consider our salinity-corrected reconstructions as a first-order sensitivity test to evaluate the potential bias in B/Ca records. While regional salinity variations can account for some minor differences between B/Ca anomalies among studied sites, ultimately the trends remain robust and most consistent with ocean carbonate chemistry as the main driver of PETM B/Ca records.

(d) Impact of preservation

With multiple sites from a diverse range of palaeoceanographic settings, palaeodepths, sediment burial depths, lithology and diagenetic pathways, we can assess the potential impact of preservation on individual boron proxy records. Differential dissolution tends to lower B/Ca of surface planktonic foraminifera [60], but shows little impact on thermocline dwellers [61]. It was

speculated that variable dissolution response between species is the result of heterogeneous B distribution within the test and relatively greater dissolution susceptibility of certain test textures [61]. δ^{11}B of *T. sacculifer* was found to lower with increasing water depth, again as a result of enhanced dissolution [62–64]. However, δ^{11}B in *Globigerinoides ruber* does not follow a similar dissolution pattern [63,64]. This variable dissolution susceptibility between different species is argued to be a result of differential δ^{11}B heterogeneity within the test or variable dissolution susceptibility of ontogenetic versus gametogenic calcite [65]. The proximity of sites 689 (1100 m) and 690 (1900 m) but with different palaeo water depths provides a scenario to test a depth-related dissolution influence on B/Ca. The close similarity of the absolute values and trends in sites 689 and 690 B/Ca records despite disparate palaeodepths suggests a minimal and consistent influence of dissolution (figure 2*b*,*c*).

An additional opportunity to assess the foraminiferal preservation state comes with the strontium/calcium ratio (Sr/Ca) of biogenic $CaCO_3$, which is released into pore fluids during calcite dissolution and excluded during inorganic calcite precipitation. Indeed, detailed Sr/Ca measurements of diagenetically altered foraminiferal calcite show lower values, clearly demonstrating the effect of dissolution and recrystallization [66]. Sr/Ca values at Bass River and Ancora are generally higher than the value typical of diagenetic calcite (1.0 mmol mol^{-1}) [66], indicating that diagenesis did not compromise the geochemical records, with the exception of samples within two discrete depth intervals not included in the reconstructions [11]. Foraminiferal Sr/Ca at site 1209 is lower (near 1 mmol mol^{-1} [42]), consistent with the 'frosty' texture of foraminifers at that site. However, Sr/Ca is near constant throughout the PETM interval, suggesting that if recrystallization has altered foraminiferal trace element compositions it has done so uniformly over this short time interval and, therefore, relative changes in B/Ca should be preserved.

Another strategy to evaluate the effects of preservation on geochemical signals is to compare sites with identical environmental conditions but demonstrably different diagenetic sediment histories. Edgar *et al*. [65] compared time-equivalent (Middle Eocene) planktonic foraminiferal B/Ca and δ^{11}B records from glassy foraminifers (Tanzanian Drilling Project, Indian Ocean) with a site that contains recrystallized foraminifera (ODP 865, central Pacific Ocean). Planktonic foraminiferal B/Ca are lower in the recrystallized (frosty) foraminifers from site 865, yet, by contrast, δ^{11}B values were similar, suggesting that exchange between pore fluids and recrystallized carbonate can result in a lowering of boron concentration without isotopic fractionation. This predicts that B/Ca in diagenetically precipitated inorganic calcite is lower than biogenic calcite, which is consistent with the idea of preferential B exclusion during recrystallization. While this raises some concern for the pelagic records, site 865 represents an extreme example of recrystallization as the entire sediment column consists of a high-porosity ooze dominated by foraminifera sand so that recrystallization is occurring in a completely or partially open system at high seawater to $CaCO_3$ ratios [67]. This contrasts with the lower porosity pelagic sites in this study, where pore water chemistry is mainly controlled by diffusion and diagenesis occurs in a relatively closed system at lower seawater to $CaCO_3$ ratios. Furthermore, the continental shelf sites (sites Bass River and Ancora) exhibit exceptionally well-preserved foraminifera with classic glassy shell textures similar to the preservation seen in Eocene Tanzania sections [68]. The relatively impermeable nature of clay-rich sediments limits or even prevents interaction of foraminiferal calcite with pore fluids, thus preserving primary chemical signatures. Visual evaluation of the site Bass River foraminifera by scanning electron microscopy supports this claim [11]. Remarkably, despite these different diagenetic histories and preservation states between the shelf and pelagic sites, a similar pattern of B/Ca is recorded, suggesting that any diagenetic bias on relative trends of individual records is minimal (figure 2*a*–*c*).

(e) Symbiont loss

A potential biological consequence of warming is loss of photosymbionts (bleaching) in planktonic foraminifera. Evidence of symbiont bleaching in planktonic foraminifera was

previously suggested for the Middle Eocene [69,70]. Since the early stages of δ^{11}B proxy development, it was apparent that biogenic $CaCO_3$ is likely not to be simply a recorder of ambient seawater pH but also carries the signal of local pH variation within the calcifying microenvironment. Physiological processes including symbiont photosynthesis, respiration and calcification can modify local pH [71,72] and, in turn, B/Ca and δ^{11}B of foraminiferal calcite [73,74]. Detailed intra-test measurements in symbiont-bearing benthic foraminifera [75], light intensity in planktonic foraminifera culture experiments [53,73] and sediment-trap work [76] collectively substantiate the potential impact of symbiont activity on B/Ca and δ^{11}B.

Test size δ^{13}C gradients in PETM planktonic foraminifera taxa are used as an indicator of photosymbiont activity [45] and loss of gradients as a proxy for bleaching in symbiont-bearing species [70]. Preferential use of light carbon (^{12}C) during photosynthesis in combination with either increased photosymbiont abundance or activity in larger individuals can explain the positive relationship between test size and δ^{13}C. The δ^{13}C test size gradients in symbiont-bearing species (*A. soldadoensis* and *Morozovella* spp.) in shelf sites are maintained within the CIE, suggesting that, at temperate latitudes, bleaching did not occur [11]. Deeper dwelling *Subbotina* spp. also record a B/Ca and δ^{11}B change, corroborating the trends shown in symbiotic surface dwellers within the same cores, signifying that even if bleaching did occur it cannot explain the entire signal (figures 2*a–c* and 3). In addition, Southern Ocean sites (689, 690) were located in comparatively colder polar waters where foraminifera would presumably be less vulnerable to warming-induced bleaching. The close similarity of the B/Ca trends between the cold high latitudes (sites 689 and 690), the warm low latitudes (site 1209), and the temperate continental shelf (NJ margin) argues against symbiont bleaching as a major driver of the B/Ca trends at all sites.

(f) Biological implications

Our global compilation of boron proxy (δ^{11}B and B/Ca) reconstructions reveals near-uniform upper ocean acidification (figures 3*c* and 4). The similarity in B/Ca values between records implies minimal spatial variability in absolute ocean carbonate chemistry (e.g. [B(OH)$_4^-$/DIC]) (figure 4). Since the degree of acidification was uniformly expressed in the surface ocean then there appears to be no refuge. The carbonate saturation state, on the other hand, could be spatially variable, which is suggested during the PETM by model output [77]. However, if we follow this logic, the high latitudes would be closer to undersaturated values with respect to $CaCO_3$ and thus are more vulnerable to acidification. There could be short-term responses to ocean acidification during the CIE onset that are not captured in our B proxy records, as dissolution gaps at the CIE onset are common in most sections, even in the shallow marine shelf sections. Another possibility is that the combined effects of ocean acidification and warming on marine biota could be more significant than ocean carbonate chemistry as an independent stressor.

Several major plankton groups experienced dynamic changes during the PETM, including evolutionary turnover and shifts in latitudinal distribution, probably in response to warming. Moreover, geochemical evidence indicates that tropical sea-surface temperatures probably exceeded 30°C, thereby pushing thermal thresholds observed in the modern ocean [78,79]. In the tropics, mixed-layer dwelling planktonic foraminifera (morozovellids and acarininids) exhibit a transient increase in morphological variation that included the appearance of distinctive (malformed) ecophenotypes, whereas populations of thermocline-dwelling taxa (subbotinids) temporarily collapsed at some locations [80]. A similar pattern of migration and elevated levels of taxonomic turnover is also observed in calcareous nannoplankton [81], *Apectodinium* spp. dinocysts [82] and radiolarians [83]. These lines of evidence are consistent with the heterogeneous latitudinal pattern of ocean warming [7].

There is a wealth of evidence implicating warming as an agent of change amongst plankton communities, yet the high incidence of malformed nannoplankton and thinning of coccolithophores found at numerous sites during the peak of the CIE suggests that ocean acidification also played a role [84–87]. Still, the impact of undersaturation on nannoplankton

was exceeded by that of temperature; extracellular coccolithophore groups thought to be sensitive to ocean chemistry took refuge in cool waters at high latitudes [77]. Moreover, increased rates of coccoliths and foraminifera malformation in coastal sites suggest that the pH decline in combination with warming and eutrophication increased stress on planktonic calcifiers [88]. A similar combination of stressors was previously suggested for the collapse of framework-building corals during the PETM [89]. Disentangling the biotic effects of multiple abiotic stressors is proving to be a challenging task and should be a focus of future research. Nevertheless, the relative impacts of future ocean acidification are likely to be more severe as anthropogenic emission rates are considerably faster than estimated for the PETM [12,90,91].

5. Conclusion

The similarities between foraminiferal boron proxy records over the PETM, from a variety of palaeoceanographic settings and diagenetic histories, is consistent with globally uniform ocean acidification as the primary driver for the first-order feature common to all records: the large, rapid decrease in B/Ca and δ^{11}B at the onset of the CIE. Subtle differences in absolute values between sites can be explained by differences in local oceanographic conditions, including salinity and dissolution. The boron isotope records at several of our sites allow us to quantify the degree of ocean acidification and suggest approximately a 0.15–0.3 pH unit decrease in the upper ocean. These estimates overlap with the higher end of carbon emissions scenarios considered in carbon cycle model simulations of the event [14,15]. This degree of acidification is less severe than the 0.4 pH unit decrease predicted for the end of the twenty-first century due to anthropogenic carbon emissions [92] and probably occurred over several thousand years [90,91], an order of magnitude slower than current ocean acidification. This might explain the general lack of extinctions among mixed-layer dwelling calcifiers during the PETM.

Finally, all boron records indicate a prolonged state of moderate acidification lasting as long as the CIE, adding to the mounting evidence (including the 'body' of the CIE itself [15] and a delayed CCD overshoot [31]) that carbon emissions continued for several tens of thousands of years following the onset of the PETM.

References

1. McInerney FA, Wing SL. 2011 The Paleocene-Eocene thermal maximum: a perturbation of carbon cycle, climate, and biosphere with implications for the future. *Annu. Rev. Earth Planet. Sci.* **39**, 489–516. (doi:10.1146/annurev-earth-040610-133431)
2. Kennett JP, Stott LD. 1991 Abrupt deep-sea warming, paleoceanographic changes and benthic extinctions at the end of the Paleocene. *Nature* **353**, 225–229. (doi:10.1038/353225a0)

3. Koch PL, Zachos JC, Gingerich PD. 1992 Correlation between isotope records in marine and continental carbon reservoirs near the Palaeocene/Eocene boundary. *Nature* **358**, 319–322. (doi:10.1038/358319a0)

4. Dickens GR, Castillo MM, Walker JCG. 1997 A blast of gas in the latest Paleocene: simulating first-order effects of massive dissociation of oceanic methane hydrate. *Geology* **25**, 259–262. (doi:10.1130/0091-7613(1997)025<0259:abogit>2.3.co;2)

5. Caldeira K, Wickett ME. 2003 Anthropogenic carbon and ocean pH. *Nature* **425**, 365. (doi:10.1038/425365a)

6. Gruber N. 2011 Warming up, turning sour, losing breath: ocean biogeochemistry under global change. *Phil. Trans. R. Soc. A* **369**, 1980–1996. (doi:10.1098/rsta.2011.0003)

7. Dunkley Jones T, Lunt DJ, Schmidt DN, Ridgwell A, Sluijs A, Valdes PJ, Maslin M. 2013 Climate model and proxy data constraints on ocean warming across the Paleocene–Eocene Thermal Maximum. *Earth Sci. Rev.* **125**, 123–145. (doi:10.1016/j.earscirev.2013.07.004)

8. Zachos JC *et al.* 2005 Rapid acidification of the ocean during the Paleocene-Eocene Thermal Maximum. *Science* **308**, 1611–1615. (doi:10.1126/science.1109004)

9. Colosimo AB, BralowerTJ, Zachos JC. 2006 Evidence for lysocline shoaling and methane hydrate dissociation at the Paleocene-Eocene Thermal Maximum on Shatsky Rise, ODP Leg 198. In *Proc. of the Ocean Drilling Program, scientific results* (eds TJ Bralower, I Premoli Silva, M Malone), pp. 1–36. College Station, TX: Ocean Drilling Program.

10. Penman DE, Hönisch B, Zeebe RE, Thomas E, Zachos JC. 2014 Rapid and sustained surface ocean acidification during the Paleocene-Eocene Thermal Maximum. *Paleoceanography* **29**, 2014PA002621. (doi:10.1002/2014PA002621)

11. Babila TL, Rosenthal Y, Wright JD, Miller KG. 2016 A continental shelf perspective of ocean acidification and temperature evolution during the Paleocene-Eocene Thermal Maximum. *Geology* **44**, 275–278. (doi:10.1130/g37522.1)

12. Gutjahr M, Ridgwell A, Sexton PF, Anagnostou E, Pearson PN, Pälike H, Norris RD, Thomas E, Foster GL. 2017 Very large release of mostly volcanic carbon during the Palaeocene–Eocene Thermal Maximum. *Nature* **548**, 573. (doi:10.1038/nature23646)

13. Panchuk K, Ridgwell A, Kump LR. 2008 Sedimentary response to Paleocene-Eocene Thermal Maximum carbon release: a model-data comparison. *Geology* **36**, 315–318. (doi:10.1130/g24474a.1)

14. Ridgwell A, Schmidt DN. 2010 Past constraints on the vulnerability of marine calcifiers to massive carbon dioxide release. *Nat. Geosci.* **3**, 196–200. (doi:10.1038/ngeo755)

15. Zeebe RE, Zachos JC, Dickens GR. 2009 Carbon dioxide forcing alone insufficient to explain Palaeocene-Eocene Thermal Maximum warming. *Nat. Geosci.* **2**, 576–580. (doi:10.1038/ngeo578)

16. Thomas E. 2007 Cenozoic mass extinctions in the deep sea: what perturbs the largest habitat on Earth? *Geol. Soc. Am. Spec. Pap.* **424**, 1–23. (doi:10.1130/2007.2424(01))

17. Thomas E. 1998 Biogeography of the Late Paleocene Benthic foraminiferal extinction. In *Late Paleocene-Early Eocene climatic and biotic events in the marine and terrestrial records* (eds M-P Aubry, SG Lucas, WA Berggren), pp. 214–234. New York, NY: Columbia University Press.

18. Kelly DC, Nielsen TMJ, Schellenberg SA. 2012 Carbonate saturation dynamics during the Paleocene–Eocene Thermal Maximum: bathyal constraints from ODP sites 689 and 690 in the Weddell Sea (South Atlantic). *Mar. Geol.* **303–306**, 75–86. (doi:10.1016/j.margeo.2012.02.003)

19. Kelly DC. 2002 Response of Antarctic (ODP Site 690) planktonic foraminifera to the Paleocene–Eocene Thermal Maximum: faunal evidence for ocean/climate change. *Paleoceanography* **17**, 23-1–23-13. (doi:10.1029/2002pa000761)

20. Miller KG *et al.* 1999 Ancora site. In *Proc. of the Ocean Drilling Program, Initial Reports 174AX* (eds KG Miller, PJ Sugarman, JV Browning *et al.*), pp. 1–65. College Station, TX: Ocean Drilling Program.

21. Miller KG *et al.* 1998 Bass River site. In *Proc. of the Ocean Drilling Program, Initial Reports 174AX* (eds KG Miller, PJ Sugarman, JV Browning *et al.*), pp. 5–43. College Station, TX: Ocean Drilling Program.

22. Sugarman PJ *et al.* 2005 Millville site. In *Proc. of the Ocean Drilling Program, Initial Reports 174AX* (eds KG Miller, PJ Sugarman, JV Browning *et al.*), pp. 1–94. College Station, TX: Ocean Drilling Program.

23. Harris AD, Miller KG, Browning JV, Sugarman PJ, Olsson RK, Cramer BS, Wright JD. 2010 Integrated stratigraphic studies of Paleocene-lowermost Eocene sequences, New

Jersey Coastal Plain: evidence for glacioeustatic control. *Paleoceanography* **25**, PA3211. (doi:10.1029/2009pa001800)

24. Stassen P, Thomas E, Speijer RP. 2012 Integrated stratigraphy of the Paleocene-Eocene Thermal Maximum in the New Jersey Coastal Plain: toward understanding the effects of global warming in a shelf environment. *Paleoceanography* **27**, PA4210. (doi:10.1029/2012PA002323)

25. Bains S, Corfield RM, Norris RD. 1999 Mechanisms of climate warming at the end of the Paleocene. *Science* **285**, 724–727. (doi:10.1126/science.285.5428.724)

26. John CM, Bohaty SM, Zachos JC, Sluijs A, Gibbs S, Brinkhuis H, Bralower TJ. 2008 North American continental margin records of the Paleocene-Eocene Thermal Maximum: implications for global carbon and hydrological cycling. *Paleoceanography* **23**, A2217. (doi:10.1029/2007pa001465)

27. Makarova M, Wright JD, Miller KG, Babila TL, Rosenthal Y, Park JI. 2017 Hydrographic and ecologic implications of foraminiferal stable isotopic response across the U.S. mid-Atlantic continental shelf during the Paleocene-Eocene Thermal Maximum. *Paleoceanography* **32**, 56–73. (doi:10.1002/2016PA002985)

28. Henehan MJ, Foster GL, Bostock HC, Greenop R, Marshall BJ, Wilson PA. 2016 A new boron isotope-pH calibration for *Orbulina universa*, with implications for understanding and accounting for 'vital effects'. *Earth Planet. Sci. Lett.* **454**, 282–292. (doi:10.1016/j.epsl.2016.09.024)

29. Bowen GJ, Zachos JC. 2010 Rapid carbon sequestration at the termination of the Palaeocene–Eocene Thermal Maximum. *Nat. Geosci.* **3**, 866. (doi:10.1038/ngeo1014)

30. Kelly DC, Nielsen TMJ, McCarren HK, Zachos JC, Röhl U. 2010 Spatiotemporal patterns of carbonate sedimentation in the South Atlantic: implications for carbon cycling during the Paleocene–Eocene Thermal Maximum. *Palaeogeogr. Palaeoclimatol. Palaeoecol.* **293**, 30–40. (doi:10.1016/j.palaeo.2010.04.027)

31. Penman DE *et al.* 2016 An abyssal carbonate compensation depth overshoot in the aftermath of the Palaeocene-Eocene Thermal Maximum. *Nat. Geosci.* **9**, 575–580. (doi:10.1038/ngeo2757)

32. Luo Y, Boudreau BP, Dickens GR, Sluijs A, Middelburg JJ. 2016 An alternative model for $CaCO_3$ over-shooting during the PETM: biological carbonate compensation. *Earth Planet. Sci. Lett.* **453**, 223–233. (doi:10.1016/j.epsl.2016.08.012)

33. Bornemann A, Norris RD, Lyman JA, D'Haenens S, Groeneveld J, Röhl U, Farley KA, Speijer RP. 2014 Persistent environmental change after the Paleocene–Eocene Thermal Maximum in the eastern North Atlantic. *Earth Planet. Sci. Lett.* **394**, 70–81. (doi:10.1016/j.epsl.2014.03.017)

34. Party SS. 1979 Site 401. In *Initial reports of the deep sea drilling project* (eds L Montadert, DG Roberts), pp. 77–123. Washington, DC: U.S. Government Printing Office.

35. Zeebe RE, Zachos JC. 2007 Reversed deep-sea carbonate ion basin gradient during Paleocene-Eocene Thermal Maximum. *Paleoceanography* **22**, PA3201. (doi:10.1029/2006pa001395)

36. Zachos JC *et al.* 2004 Leg 208. In *Proc. of the Ocean Drilling Program, Initial Reports*. College Station, TX: Ocean Drilling Program.

37. Klochko K, Kaufman AJ, Yao W, Byrne RH, Tossell JA. 2006 Experimental measurement of boron isotope fractionation in seawater. *Earth Planet. Sci. Lett.* **248**, 276–285. (doi:10.1016/j.epsl.2006.05.034)

38. Anagnostou E, John EH, Edgar KM, Foster GL, Ridgwell A, Inglis GN, Pancost RD, Lunt DJ, Pearson PN. 2016 Changing atmospheric CO2 concentration was the primary driver of early Cenozoic climate. *Nature* **533**, 380–384. (doi:10.1038/nature17423)

39. Hain MP, Sigman DM, Higgins JA, Haug GH. 2015 The effects of secular calcium and magnesium concentration changes on the thermodynamics of seawater acid/base chemistry: implications for Eocene and Cretaceous ocean carbon chemistry and buffering. *Glob. Biogeochem. Cycles* **29**, 517–533. (doi:10.1002/2014GB004986)

40. Anand P, Elderfield H, Conte MH. 2003 Calibration of Mg/Ca thermometry in planktonic foraminifera from a sediment trap time series. *Paleoceanography* **18**, 15 PA1050. (doi:10.1029/2002pa000846)

41. Evans D, Müller W. 2012 Deep time foraminifera Mg/Ca paleothermometry: nonlinear correction for secular change in seawater Mg/Ca. *Paleoceanography* **27**, PA4205. (doi:10.1029/2012PA002315)

42. Zachos JC, Wara MW, Bohaty S, Delaney ML, Petrizzo MR, Brill A, Bralower TJ, Premoli-Silva I. 2003 A transient rise in tropical sea surface temperature during the Paleocene-Eocene Thermal Maximum. *Science* **302**, 1551–1554. (doi:10.1126/science.1090110)

43. Kiehl JT, Shields CA. 2013 Sensitivity of the Palaeocene–Eocene Thermal Maximum climate to cloud properties. *Phil. Trans. R. Soc. A* **371**, 20130093. (doi:10.1098/rsta.2013.0093)

44. Foster GL, Rae JWB. 2016 Reconstructing ocean pH with boron isotopes in foraminifera. *Annu. Rev. Earth Planet. Sci.* **44**, 207–237. (doi:10.1146/annurev-earth-060115-012226)

45. D'Hondt S, Zachos JC, Schultz G. 1994 Stable isotopic signals and photosymbiosis in Late Paleocene planktic foraminifera. *Paleobiology* **20**, 391–406. (doi:10.1017/S0094837300012847)

46. Birch HS, Coxall HK, Pearson PN. 2012 Evolutionary ecology of Early Paleocene planktonic foraminifera: size, depth habitat and symbiosis. *Paleobiology* **38**, 374–390. (doi:10.1666/11027.1)

47. Quillévéré F, Norris RD, Moussa I, Berggren WA. 2001 Role of photosymbiosis and biogeography in the diversification of Early Paleogene Acarininids (Planktonic Foraminifera). *Paleobiology* **27**, 311–326. (doi:10.1666/0094-8373(2001)027<0311:ROPABI>2.0.CO;2)

48. Pearson PN, Palmer MR. 1999 Middle Eocene seawater pH and atmospheric carbon dioxide concentrations. *Science* **284**, 1824–1826. (doi:10.1126/science.284.5421.1824)

49. Sanyal A, Bijma J, Spero H, Lea DW. 2001 Empirical relationship between pH and the boron isotopic composition of *Globigerinoides sacculifer*: implications for the boron isotope paleo-pH proxy. *Paleoceanography* **16**, 515–519. (doi:10.1029/2000PA000547)

50. Allen KA, Hönisch B, Eggins SM, Rosenthal Y. 2012 Environmental controls on B/Ca in calcite tests of the tropical planktic foraminifer species *Globigerinoides ruber* and *Globigerinoides sacculifer*. *Earth Planet. Sci. Lett.* **351–352**, 270–280. (doi:10.1016/j.epsl.2012.07.004)

51. Henehan MJ, Foster GL, Rae JWB, Prentice KC, Erez J, Bostock HC, Marshall BJ, Wilson PA. 2015 Evaluating the utility of B/Ca ratios in planktic foraminifera as a proxy for the carbonate system: a case study of Globigerinoides ruber. *Geochem. Geophys. Geosyst.* **16**, 1052–1069. (doi:10.1002/2014GC005514))

52. Howes EL, Kaczmarek K, Raitzsch M, Mewes A, Bijma N, Horn I, Misra S, Gattuso JP, Bijma J. 2017 Decoupled carbonate chemistry controls on the incorporation of boron into *Orbulina universa*. *Biogeosciences* **14**, 415–430. (doi:10.5194/bg-14-415-2017)

53. Haynes LL, Hönisch B, Dyez KA, Holland K, Rosenthal Y, Fish CR, Subhas AV, Rae JWB. 2017 Calibration of the B/Ca proxy in the planktic foraminifer *Orbulina universa* to Paleocene seawater conditions. *Paleoceanography* **32**, 580–599. (doi:10.1002/2016PA003069)

54. Thomas DJ, Zachos JC, Bralower TJ, Thomas E, Bohaty S. 2002 Warming the fuel for the fire: evidence for the thermal dissociation of methane hydrate during the Paleocene-Eocene Thermal Maximum. *Geology* **30**, 1067–1070. (doi:10.1130/0091-7613(2002)030<1067:WTFFTF>2.0.CO;2)

55. Bemis BE, Spero HJ, Bijma J, Lea DW. 1998 Reevaluation of the oxygen isotopic composition of planktonic foraminifera: experimental results and revised paleotemperature equations. *Paleoceanography* **13**, 150–160. (doi:10.1029/98pa00070)

56. Zachos JC, Schouten S, Bohaty S, Quattlebaum T, Sluijs A, Brinkhuis H, Gibbs SJ, Bralower TJ. 2006 Extreme warming of mid-latitude coastal ocean during the Paleocene-Eocene Thermal Maximum: inferences from TEX86 and isotope data. *Geology* **34**, 737–740. (doi:10.1130/g22522.1)

57. Ostland GH. 1987 GEOSECS Atlantic, Pacific and Indian Ocean expeditions. Shorebased data and graphica. *GEOSECS Atlas Ser.* **7**, 200.

58. Mackensen A, Hubberten H-W, Scheele N, Schlitzer R. 1996 Decoupling of $\delta^{13}C_{\sum CO2}$ and phosphate in recent Weddell Sea deep and bottom water: implications for glacial Southern Ocean paleoceanography. *Paleoceanography* **11**, 203–215. (doi:10.1029/95PA03840)

59. LeGrande AN, Schmidt GA. 2006 Global gridded data set of the oxygen isotopic composition in seawater. *Geophys. Res. Lett.* **33**, L12604. (doi:10.1029/2006gl026011)

60. Coadic R, Bassinot F, Dissard D, Douville E, Greaves M, Michel E. 2013 A core-top study of dissolution effect on B/Ca in *Globigerinoides sacculifer* from the tropical Atlantic: potential bias for paleo-reconstruction of seawater carbonate chemistry. *Geochem. Geophys. Geosyst.* **14**, 1053–1068. (doi:10.1029/2012GC004296)

61. Dai Y, Yu J, Johnstone HJH. 2016 Distinct responses of planktonic foraminiferal B/Ca to dissolution on seafloor. *Geochem. Geophys. Geosyst.* **17**, 1339–1348. (doi:10.1002/2015GC006199)

62. Hönisch B, Hemming NG. 2004 Ground-truthing the boron isotope-paleo-pH proxy in planktonic foraminifera shells: partial dissolution and shell size effects. *Paleoceanography* **19**, 13 PA4010. (doi:10.1029/2004PA001026)

63. Ni Y, Foster GL, Bailey T, Elliott T, Schmidt DN, Pearson P, Haley B, Coath C. 2007 A core top assessment of proxies for the ocean carbonate system in surface-dwelling foraminifers. *Paleoceanography* **22**, PA3212. (doi:10.1029/2006PA001337)

64. Seki O, Foster GL, Schmidt DN, Mackensen A, Kawamura K, Pancost RD. 2010 Alkenone and boron-based Pliocene pCO2 records. *Earth Planet. Sci. Lett.* **292**, 201–211. (doi:10.1016/j.epsl.2010.01.037)

65. Edgar KM, Anagnostou E, Pearson PN, Foster GL. 2015 Assessing the impact of diagenesis on δ11B, δ13C, δ18O, Sr/Ca and B/Ca values in fossil planktic foraminiferal calcite. *Geochim. Cosmochim. Acta* **166**, 189–209. (doi:10.1016/j.gca.2015.06.018)

66. Kozdon R, Kelly DC, Kitajima K, Strickland A, Fournelle JH, Valley JW. 2013 In situ δ18O and Mg/Ca analyses of diagenetic and planktic foraminiferal calcite preserved in a deep-sea record of the Paleocene-Eocene Thermal Maximum. *Paleoceanography* **28**, 517–528. (doi:10.1002/palo.20048)

67. Party SS. 1993 Site 865. In *Proceedings of the Ocean Drilling Program, Initial Reports 143* (eds WW Sager, EL Winterer, JV Firth, SS Party), pp. 111–180. College Station, TX: Ocean Drilling Program.

68. Pearson PN, Ditchfield PW, Singano J, Harcourt-Brown KG, Nicholas CJ, Olsson RK, Shackleton NJ, Hall MA. 2001 Warm tropical sea surface temperatures in the Late Cretaceous and Eocene epochs. *Nature* **413**, 481–487. (doi:10.1038/35097000)

69. Wade B, Al-Sabouni N, Hemleben C, Kroon D. 2008 Symbiont bleaching in fossil planktonic foraminifera. *Evol. Ecol.* **22**, 253–265. (doi:10.1007/s10682-007-9176-6)

70. Edgar KM, Bohaty SM, Gibbs SJ, Sexton PF, Norris RD, Wilson PA. 2012 Symbiont 'bleaching' in planktic foraminifera during the Middle Eocene Climatic Optimum. *Geology* **41**, 15–18. (doi:10.1130/g33388.1))

71. Rink S, Kühl M, Bijma J, Spero HJ. 1998 Microsensor studies of photosynthesis and respiration in the symbiotic foraminifer *Orbulina universa*. *Mar. Biol.* **131**, 583–595. (doi:10.1007/s002270050350)

72. Jørgensen BB, Erez J, Revsbech NP, Cohe Y. 1985 Symbiotic photosynthesis in a planktonic foraminiferan, *Globeriginoides sacculifer* (Brady), studied with microelectrodes. *Limnol. Oceanogr.* **30**, 1253–1267. (doi:10.4319/lo.1985.30.6.1253)

73. Hönisch B, Bijma J, Russell AD, Spero HJ, Palmer MR, Zeebe RE, Eisenhauer A. 2003 The influence of symbiont photosynthesis on the boron isotopic composition of foraminifera shells. *Mar. Micropaleontol.* **49**, 87–96. (doi:10.1016/S0377-8398(03)00030-6)

74. Zeebe RE, Wolf-Gladrow DA, Bijma J, Hönisch B. 2003 Vital effects in foraminifera do not compromise the use of δ^{11}B as a paleo-pH indicator: evidence from modelling. *Paleoceanography* **18**, 1043. (doi:10.1029/2003PA000881)

75. Rollion-Bard C, Erez J. 2010 Intra-shell boron isotope ratios in the symbiont-bearing benthic foraminiferan *Amphistegina lobifera*: implications for δ^{11}B vital effects and paleo-pH reconstructions. *Geochim. Cosmochim. Acta* **74**, 1530–1536. (doi:10.1016/j.gca.2009.11.017)

76. Babila TL, Rosenthal Y, Conte MH. 2014 Evaluation of the biogeochemical controls on B/Ca of *Globigerinoides ruber* white from the Oceanic Flux Program, Bermuda. *Earth Planet. Sci. Lett.* **404**, 67–76. (doi:10.1016/j.epsl.2014.05.053)

77. Gibbs SJ, Bown PR, Ridgwell A, Young JR, Poulton AJ, O'Dea SA. 2016 Ocean warming, not acidification, controlled coccolithophore response during past greenhouse climate change. *Geology* **44**, 59–62. (doi:10.1130/g37273.1)

78. Aze T *et al.* 2014 Extreme warming of tropical waters during the Paleocene–Eocene Thermal Maximum. *Geology* **42**, 739–742. (doi:10.1130/g35637.1)

79. Frieling J, Gebhardt H, Huber M, Adekeye OA, Akande SO, Reichart G-J, Middelburg JJ, Schouten S, Sluijs A. 2017 Extreme warmth and heat-stressed plankton in the tropics during the Paleocene-Eocene Thermal Maximum. *Sci. Adv.* **3**, 1600891. (doi:10.1126/sciadv.1600891)

80. Kelly CD, Bralower TJ, Zachos JC, Silva IP, Thomas E. 1996 Rapid diversification of planktonic foraminifera in the tropical Pacific (ODP site 865) during the Late Paleocene Thermal Maximum. *Geology* **24**, 423–426. (doi:10.1130/0091-7613(1996)024<0423:rdopfi>2.3.co;2)

81. Bralower TJ. 2002 Evidence of surface water oligotrophy during the Paleocene-Eocene Thermal Maximum: nannofossil assemblage data from Ocean Drilling Program Site 690, Maud Rise, Weddell Sea. *Paleoceanography* **17**, 13-1–13-12. (doi:10.1029/2001PA000662)

82. Sluijs A *et al.* 2006 Subtropical Arctic Ocean temperatures during the Palaeocene/Eocene Thermal Maximum. *Nature* **441**, 610–613. (doi:10.1038/nature04668)

83. Hollis CJ. 2007 Radiolarian faunal turnover through the Paleocene-Eocene transition, Mead Stream, New Zealand. In *Radiolaria: siliceous plankton through time* (eds PO Baumgartner, JC Aitchison, P De Wever, S-J Jackett), pp. 79–99. Basel, Switzerland: Birkhäuser Basel.

84. Bralower TJ, Self-Trail JM. 2016 Nannoplankton malformation during the Paleocene-Eocene Thermal Maximum and its paleoecological and paleoceanographic significance. *Paleoceanography* **31**, 1423–1439. (doi:10.1002/2016PA002980)

85. Raffi I, Backman J, Zachos JC, Sluijs A. 2009 The response of calcareous nannofossil assemblages to the Paleocene Eocene Thermal Maximum at the Walvis Ridge in the South Atlantic. *Mar. Micropaleontol.* **70**, 201–212. (doi:10.1016/j.marmicro.2008.12.005)

86. Kahn A, Aubry M-P. 2004 Provincialism associated with the Paleocene/Eocene Thermal Maximum: temporal constraint. *Mar. Micropaleontol.* **52**, 117–131. (doi:10.1016/j.marmicro.2004.04.003)

87. O'Dea SA, Gibbs SJ, Bown PR, Young JR, Poulton AJ, Newsam C, Wilson PA. 2014 Coccolithophore calcification response to past ocean acidification and climate change. *Nat. Commun.* **5**, 5363. (doi:10.1038/ncomms6363)

88. Livsey CM. 2015 The planktonic foramininferal response to the Paleocene-Eocene Thermal Maximum on the Atlantic coastal plain. Masters Thesis, Pennsylvania State University, PA, USA.

89. Speijer R, Scheibner C, Stassen P, Morsi A-M. 2012 *Response of marine ecosystems to deep-time global warming: a synthesis of biotic patterns across the Paleocene-Eocene Thermal Maximum (PETM)*. *Aust J. Earth Sci.* **105**, 6–16.

90. Zeebe RE, Ridgwell A, Zachos JC. 2016 Anthropogenic carbon release rate unprecedented during the past 66 million years. *Nat. Geosci.* **9**, 325–329. (doi:10.1038/ngeo2681)

91. Kirtland Turner S, Ridgwell A. 2016 Development of a novel empirical framework for interpreting geological carbon isotope excursions, with implications for the rate of carbon injection across the PETM. *Earth Planet. Sci. Lett.* **435**, 1–13. (doi:10.1016/j.epsl.2015.11.027)

92. Gattuso J-P *et al.* 2015 Contrasting futures for ocean and society from different anthropogenic CO_2 emissions scenarios. *Science* **349**, aac4722. (doi:10.1126/science.aac4722)